Journal of Quantitative Spectroscopy & Radiative Transfer 225 (2019) 206–213

Contents lists available at ScienceDirect

Journal of Quantitative Spectroscopy & Radiative Transfer

journal homepage: www.elsevier.com/locate/jqsrt

First high–resolution comprehensive analysis of $^{72}GeH_4$ spectra in the Dyad and Pentad regions

O.N. Ulenikov[a,*], O.V. Gromova[a], E.S. Bekhtereva[a], N.I. Raspopova[a], A.V. Kuznetsov[a], M.A. Koshelev[b], I.A. Velmuzhova[c], P.G. Sennikov[c]

[a] Research School of High–Energy Physics, National Research Tomsk Polytechnic University, Tomsk 634050, Russia
[b] Institute of Applied Physics, Russian Academy of Sciences, Nizhny Novgorod 603950, Russia
[c] G.G. Devyatykh Institute of Chemistry of High Purity Substances, Russian Academy of Sciences, Nizhny Novgorod 603950, Russia

ARTICLE INFO

Article history:
Received 21 October 2018
Revised 26 December 2018
Accepted 26 December 2018
Available online 27 December 2018

Keywords:
High resolution spectrum of (72)GeH4
Line positions
Ro-vibrational energies
Spectroscopic parameters

ABSTRACT

The spectra of germane $^{72}GeH_4$ enriched up to 99.9% in the sample were recorded with high resolution (0.003 cm^{-1}) at different pressures with the Bruker IFS 125HR Fourier transform spectrometer (Nizhny Novgorod, Russia). The region of 700–4400 cm^{-1}, where the Dyad and Pentad are located, was theoretically analyzed. The 9112 transitions belonging to the seven "cold" bands (6761 transitions) of the Dyad and Pentad and to the nine "hot" Dyad–Pentad bands (2351 transitions) were assigned and analyzed with an effective hamiltonian model which takes into account the presence of resonance interactions. The obtained set of 53 fitted parameters reproduces the initial 9112 experimental line positions with a $d_{rms} = 2.44 \times 10^{-4}$ cm^{-1}.

1. Introduction

In a set of preceding papers (see Ref. [1] and references cited therein) we studied high resolution spectra of $^{73}GeH_4$, $^{74}GeH_4$, and $^{76}GeH_4$ which have been enriched up to 88.1–99.9% of abundance of separate species in a sample. In the present study we continue this analysis and focus on the $^{72}GeH_4$ isotopologue of germane.

Earlier some separate vibrational bands of $^{72}GeH_4$ have been discussed in Refs. [2–14]. In those cases, nonenriched $^{72}GeH_4$ samples were used in the experimental studies. Therefore, it was only possible to extract a limited amount of spectroscopic information from the experimental transitions (energy levels) of this isotopologue. In the present study the sample was enriched up to 99.9% in $^{72}GeH_4$. This gave us the ability to considerably extend the information about the spectroscopic properties of $^{72}GeH_4$.

2. Experimental details

Spectra of a gas sample of germane containing 99.9% of the $^{72}GeH_4$ isotopologue were registered with a Bruker IFS125HR Fourier transform spectrometer. The method of the sample preparation is similar to the method described in our previous studies for other isotopologues of germane (see [1] and references therein). Details of the present experiment are presented in Table 1. Briefly, the spectrometer was equipped with a Globar source, a KBr beam splitter and liquid nitrogen cooled mercury–cadmium telluride (MCT) and indium antimonide (InSb) detectors. The sample spectra were recorded with a resolution of 0.003 cm^{-1} (the resolution due to the maximum optical path difference) in the frequency range 700–4400 cm^{-1}. The Norton–Beer (weak) apodization function was applied. To study both strong and weak lines, spectra were recorded at significantly different pressures and optical path lengths. A single–pass 20 cm length cell and a multi–pass White cell were used. A cell was permanently connected to a gas sample vacuum system, a turbo–molecular pump, and capacitance pressure gauges covering the 10^{-3}–100 Torr range with a stated inaccuracy of 0.5% and better. The optical compartment of the spectrometer was pumped out by a mechanical pump down to 0.02 Torr (or less) and that pressure remained constant during the experiment.

The final spectra (see Figs. 1–3) were obtained by averaging about 1000 scans. In total, five spectra were recorded at different optical path lengths and pressures. Spectra were calibrated using the most intense but unsaturated and well resolved H_2O and CO_2 lines and HITRAN database line list, [15]. After calibration the standard deviation of the difference between the measured and tabulated peak positions was estimated to be 1.8×10^{-4} cm^{-1}.

* Corresponding author.
E-mail address: ulenikov@mail.ru (O.N. Ulenikov).

https://doi.org/10.1016/j.jqsrt.2018.12.036
0022-4073/

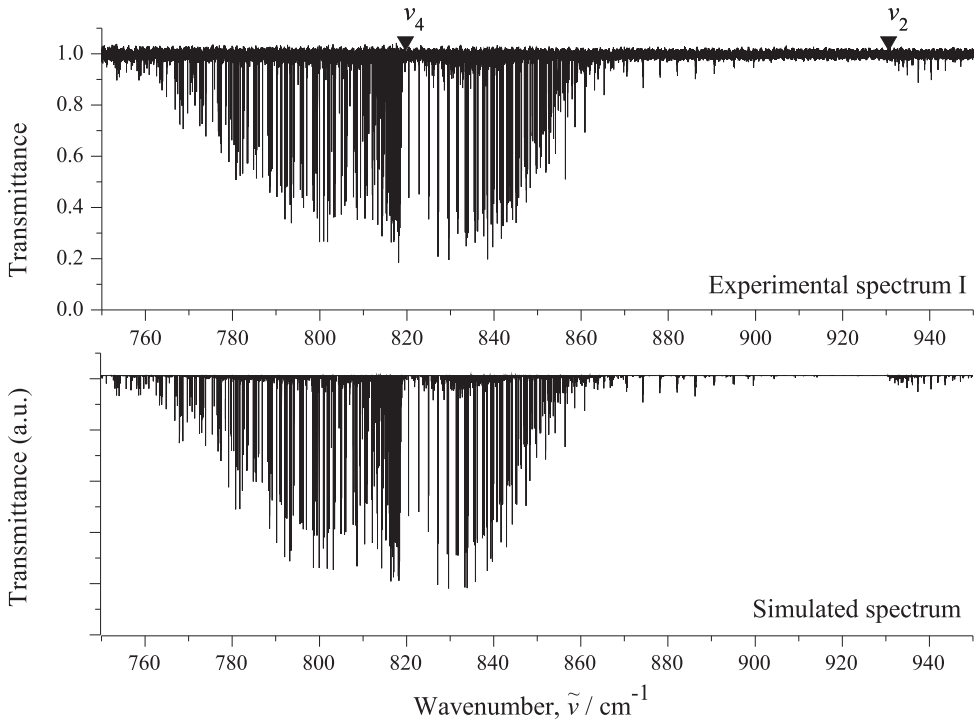

Fig. 1. Survey spectrum I of $^{72}GeH_4$ (upper trace) in the region of 750–950 cm^{-1} (for the experimental conditions, see Table 1). The bottom trace presents simulated spectrum.

Table 1
Experimental setup for the regions 700–4400 cm^{-1} of the infrared spectra of $^{72}GeH_4$.

Spectrum	Resolution /cm^{-1}	Measuring time/h	No. of scans	Spectral range /cm^{-1}	Detector	Beam-splitter	Opt. path-length/m	Aperture /mm	Temp. /°C	Pressure /Torr
I	0.003	36.9	1100	700–1930	MCT	KBr	0.2	1.7	26.4	0.04
II	0.003	33.5	1000	700–1930	MCT	KBr	0.2	1.7	25.8	4.0
III	0.003	35.2	1050	1900–4400	InSb	KBr	0.75	1.15	26.2	0.02
IV	0.003	35.2	1050	1900–4400	InSb	KBr	3.75	1.15	24.5	0.4
V	0.003	41.9	1250	1900–4400	InSb	KBr	3.75	1.15	24.2	4.0

3. Description of the spectra and assignment of transitions

The overview of the experimental spectra recorded in the regions of the Dyad (750–950 cm^{-1}, spectrum I), bending bands of the Pentad (1600–1900 cm^{-1}, spectrum II), and stretching bands of the Pentad (1925–2275 cm^{-1}, spectra III–V) of $^{72}GeH_4$ are shown in the upper parts of Figs. 1–3. In the top part of Fig. 1 one can see the clearly pronounced ν_4 band (left part of Fig. 1) and the very weak ν_2 band is seen in the right part of this figure. The $\nu_2+\nu_4(F_2)$ and $\nu_2+\nu_4(F_1)$ bands are seen in Fig. 2. Centers of the bands $2\nu_4$ and $2\nu_2$ are also marked in Fig. 2, however their rovibrational transitions cannot be seen in the experimental spectrum. Corresponding rovibrational energies of the vibrational states were determined only from the "hot" transitions (see below). The top part of Fig. 3 presents an overview of the spectra III and IV in the region of the ν_3 and ν_1 bands. Even by the way of visible inspection one can see that the experimental spectrum on the upper part of Fig. 3 contains more lines than the corresponding simulated spectrum in the bottom part of this figure. This is explained by the presence of numerous "hot" transitions from the lower (0001, F_2) and (0100, E) vibrational states to the vibrational states of the Octad. Fig. 4 b shows a small fragment of the experimental high resolution spectrum III.

The GeH_4 molecule is a spherical top with a symmetry isomorphic to the T_d point symmetry group. Transitions in absorption are allowed only between vibrational states ($v\Gamma$) and ($v'\Gamma'$) for which the relation (see, e.g., [16])

$$\Gamma \otimes \Gamma' \in F_2 \tag{1}$$

is fulfilled. Transitions between the vibrational states which do not satisfy the condition of Eq. (1) are forbidden by the symmetry of a molecule and can appear in the absorption spectra only because of resonance interactions with the allowed ones (as a consequence, usually they are considerably weaker than the allowed transitions).

At the first step of the analysis we assigned without doubt transitions belonging to the six "cold" bands: $\nu_2(E)$, $\nu_4(F_2)$, $\nu_1(A_1)$, $\nu_3(F_2)$, $\nu_2+\nu_4(F_2)$, and $\nu_2+\nu_4(F_1)$. For these six bands, the 6761 transitions up to a maximum quantum number $J^{max.}=30$ were assigned (see, for details, statistical information in Table 2). This is considerably larger than earlier studies, in particular, the recent study of Boudon et al. [14] where 897 transitions of $^{72}GeH_4$ up to $J^{max.}=25$ were assigned to the $\nu_3(F_2)$ band. The correctness of our assignments was confirmed by the use of numerous combination differences. The resulting assignments are given in the Supplementary materials I, II and III to this article.

In the second analysis step the experimental transitions were assigned for the nine "hot" Dyad–Pentad bands: $2\nu_4(A_1)-\nu_4$, $2\nu_4(E)-\nu_4$, $2\nu_4(F_2)-\nu_4$, $\nu_2+\nu_4(F_2)-\nu_2$, $\nu_2+\nu_4(F_1)-\nu_2$, $\nu_2+\nu_4(F_2)-\nu_4$, $\nu_2+\nu_4(F_1)-\nu_4$, $2\nu_2(A_1)-\nu_2$, and $2\nu_2(E)-\nu_2$. The 2351 transitions were assigned to these "hot" bands. A complete

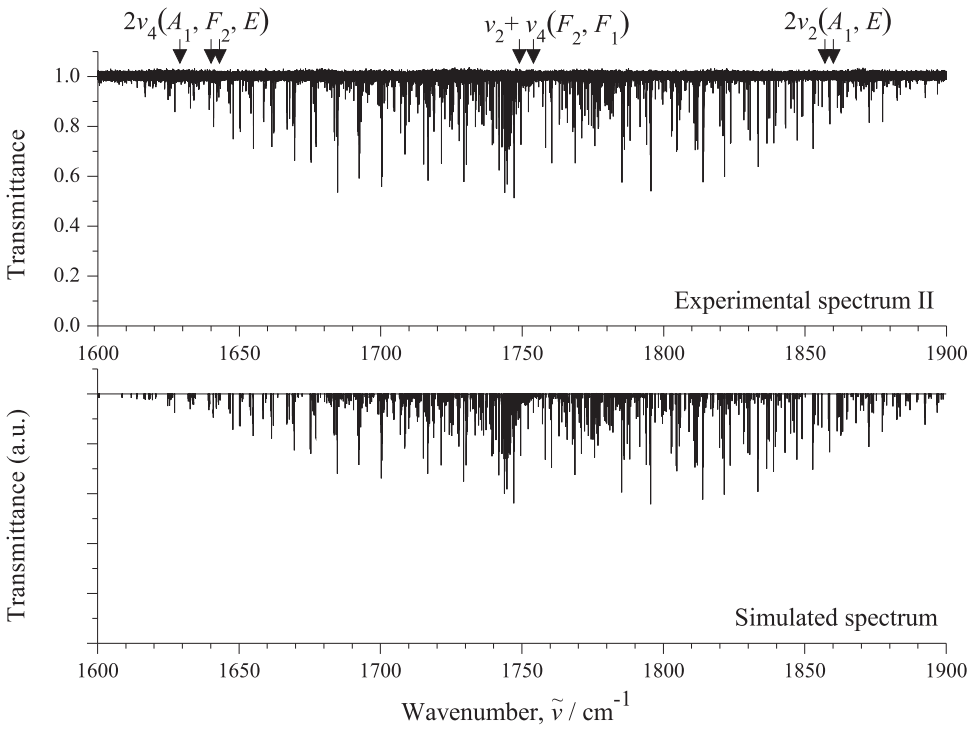

Fig. 2. Survey spectrum II of $^{72}GeH_4$ (upper trace) in the region of 1600–1900 cm^{-1} (for the experimental conditions, see Table 1). The bottom trace presents simulated spectrum.

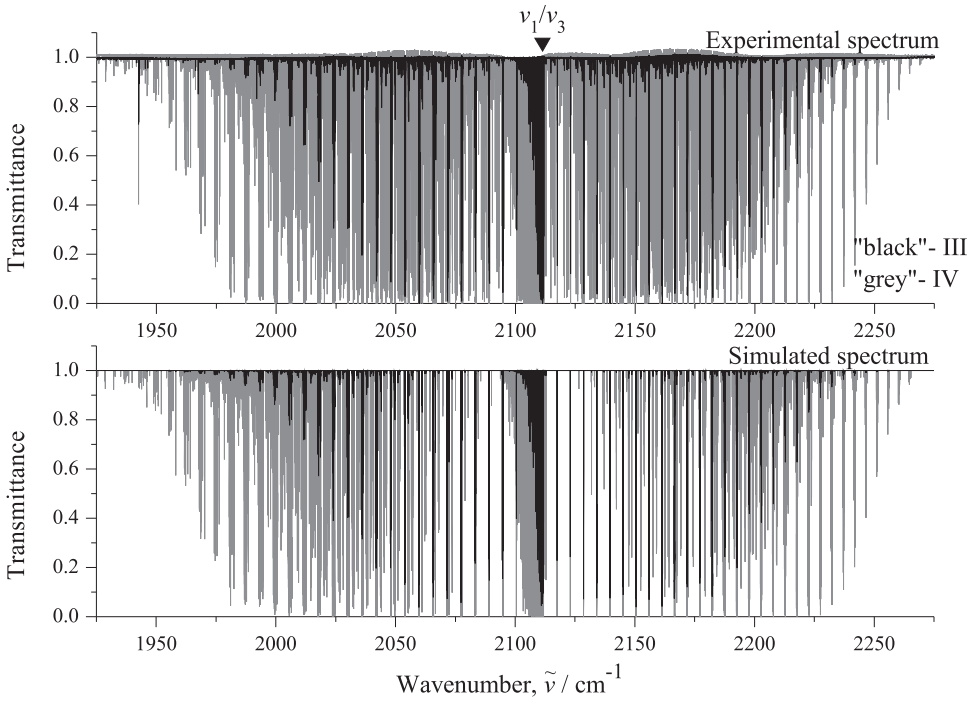

Fig. 3. Survey spectrum III and IV of $^{72}GeH_4$ (upper trace) in the region of 1925–2275 cm^{-1} (for the experimental conditions, see Table 1). The bottom trace presents simulated spectrum.

list of the "hot" assigned experimental transitions is added to the Supplementary material I (see also statistical information in Table 2). It should be mark that about 85% of transitions were assigned in the Dyad region. The remained 15% of transitions are very weak ones at the level of noise. As to the Pentad–bands region, about 65% of experimental lines were assigned, and the remained lines belong to the "hot" bands or very weak.

The above mentioned six "cold" band gave us possibility to obtain the ro-vibrational energies only for six vibrational states of the Dyad and Pentad: (0100, E), (0001, F_2), (1000, A_1), (0010,

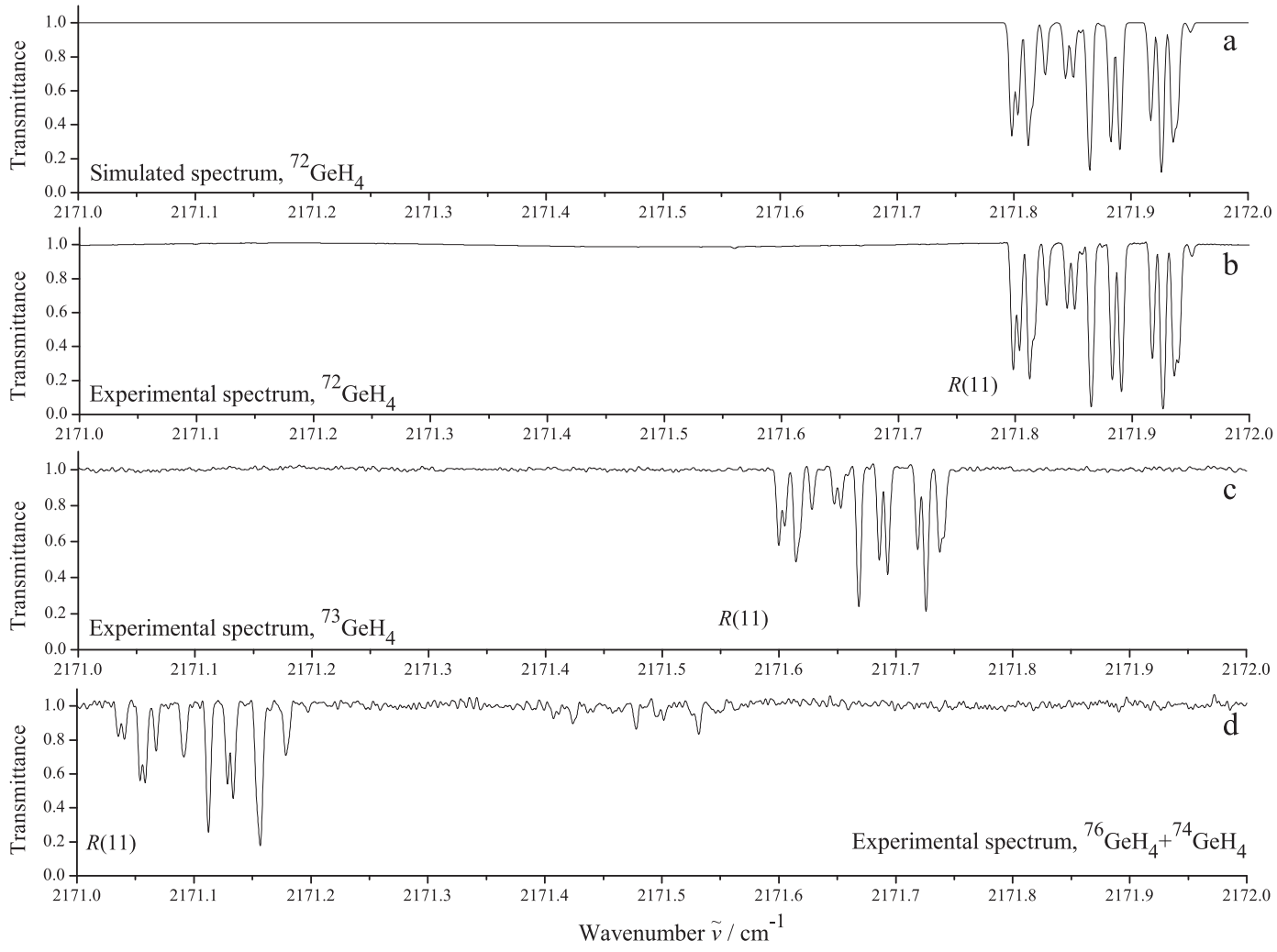

Fig. 4. Small parts of the high resolution experimental spectra of $^{72}GeH_4$ (Fig. 4b; enriched up to 99.9%), $^{73}GeH_4$ (Fig. 4; enriched up to 99.9%), and $^{74}GeH_4/^{76}GeH_4$ (Fig. 4 d; enriched up to 88.1% of $^{76}GeH_4$; abundance of $^{74}GeH_4$ is 11.5%) in the region of the R(11) cluster of the ν_3 band. The distance between analogous lines of the $^{76}GeH_4$ and $^{73}GeH_4$ isotopologues is exactly three time larger than the distance between corresponding lines of the $^{73}GeH_4$ and $^{72}GeH_4$ isotopologues. The trace 4a is the simulated spectrum of $^{72}GeH_4$.

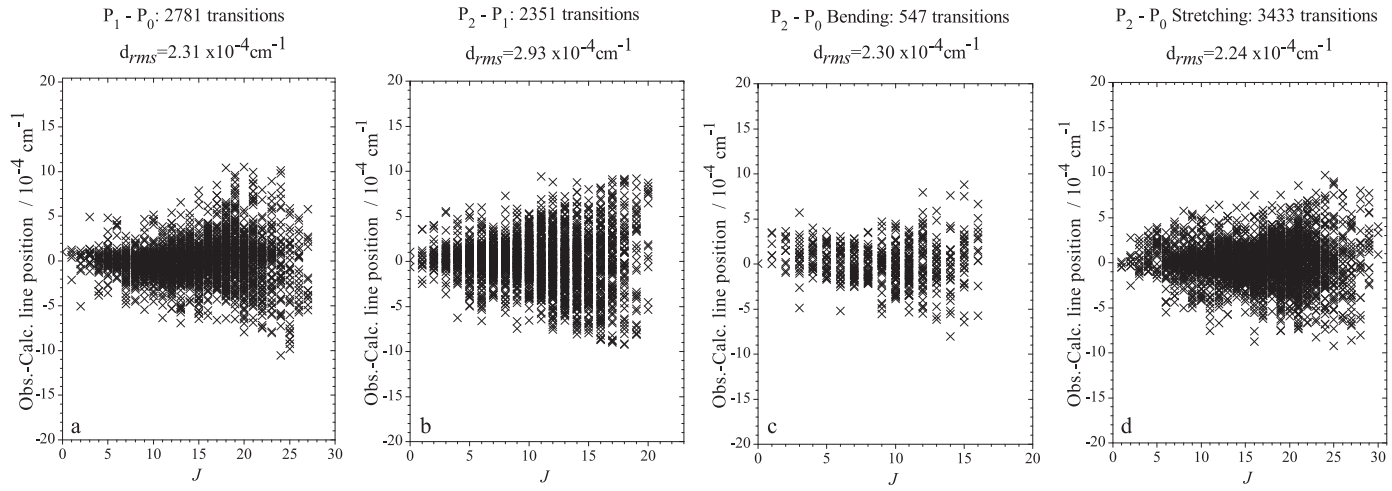

Fig. 5. Observed – calculated line positions and fit statistics for bands studied in the present paper: Fig. 5a–d correspond to the bands of the Dyad, to the "hot" bands of the Dyad–Pentad, to a set of the bending bands of the Pentad, and to the two stretching bands of the Pentad, respectively.

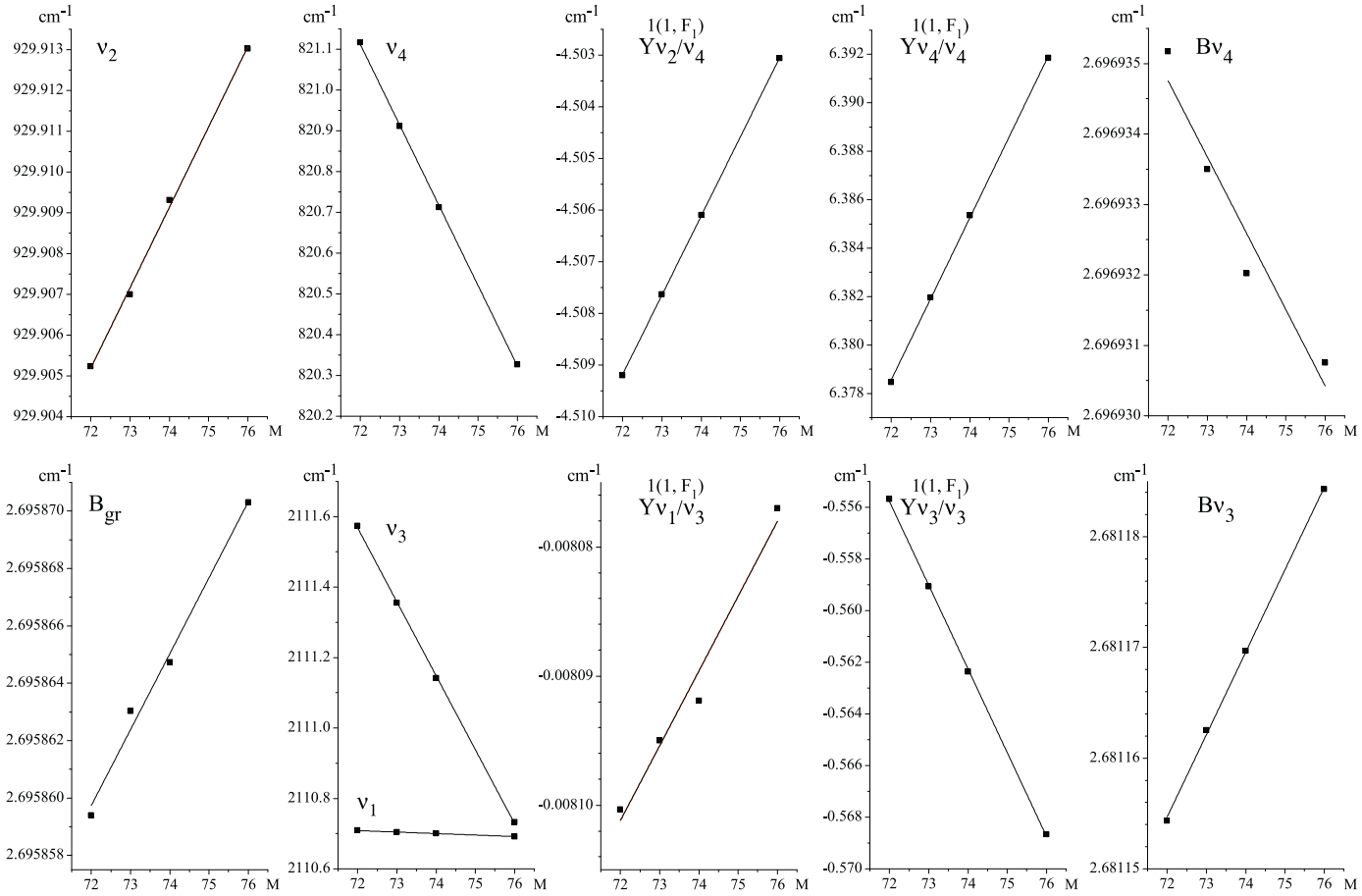

Fig. 6. Plots of the dependence of the values (in cm^{-1}) of some larger spectroscopic parameters on the mass M of the isotopic species of germane (experimental data are taken from [1] and references cited therein).

Table 2
Statistical information for the Dyad and Pentad of $^{72}GeH_4$.

Band	Center/cm^{-1}	N_{tr}[a]	J^{max}	N_{en}	m_1[b]	m_2[b]	m_3[b]
1	2	3	4	5	6	7	8
ν_4, F_2 tw[c]	821.11678	1569	27	752	78.4	14.1	7.5
ν_2, E tw[c]	929.90524	1212	26	380	79.5	14.1	6.4
ν_3, F_2 tw[c]	2111.57394	2429	30	905	76.4	16.5	7.1
ν_3, F_2 Ref. [14]	2111.57411	897	25				
ν_1, A_1 tw[c]	2110.70880	1004	28	237	80.6	15.1	4.3
$\nu_2+\nu_4$, F_2 tw[c]	1749.17866	364	16	385	73.6	20.6	5.8
$\nu_2+\nu_4$, $F_2-\nu_2$ tw[c]		400	19		70.5	19.8	9.7
$\nu_2+\nu_4$, $F_2-\nu_4$ tw[c]		146	17		67.8	19.9	12.3
$\nu_2+\nu_4$, F_1 tw[c]	1753.28969	183	16	337	78.7	16.4	4.9
$\nu_2+\nu_4$, $F_1-\nu_2$ tw[c]		406	19		69.7	19.0	11.3
$\nu_2+\nu_4$, $F_1-\nu_4$ tw[c]		82	17		68.3	28.0	3.7
$2\nu_4$, $A_1-\nu_4$ tw[c]	1629.05403	299	20	146	60.6	21.7	17.7
$2\nu_4$, $E-\nu_4$ tw[c]	1643.71586	215	20	129	60.5	23.7	15.8
$2\nu_4$, $F_2-\nu_4$ tw[c]	1640.81867	692	20	453	63.2	21.5	15.3
$2\nu_2$, $A_1-\nu_2$ tw[c]	1857.25740	5	14	5	80.0	0.0	20.0
$2\nu_2$, $E-\nu_2$ tw[c]	1860.65216	106	17	88	71.7	21.7	6.6

[a] N_{tr} is the number of assigned transitions.
[b] Here $m_i = n_i/N_{tr} \times 100\%$ (i = 1, 2, 3); n_1, n_2, and n_3 are the numbers of transitions for which the differences $\delta = \nu^{exp} - \nu^{calc}$ satisfy the conditions $\delta \leq 2 \times 10^{-4}$ cm^{-1}, 2×10^{-4} cm^{-1} $< \delta \leq 4 \times 10^{-4}$ cm^{-1}, and $\delta > 4 \times 10^{-4}$ cm^{-1}, respectively.
[c] The "tw" means "this work".

F_2), (0101, F_1) and (0101, F_2). At the same time, the presence of transitions belonging to the "hot" band, allowed us to obtain ro–vibrational energy values for the other five vibrational states of the Pentad: (0200, A_1), (0200, E), (0002, A_1), (0002, E), and (0002, F_2). In summary, 3817 ro–vibrational energy values from all eleven upper vibrational states of the Dyad and Pentad were obtained.

4. Hamiltonian model and parameters of the effective Hamiltonian

All the 3817 ro–vibrational energy values (9112 experimental transitions) discussed in the before section were used as the initial information in the weighted fit procedure to determine the spec-

Table 3
Spectroscopic parameters $Y^{\Omega(K,n\Gamma)}_{v\gamma,v'\gamma'}$ of the Dyad and Pentad of $^{72}GeH_4$ (in cm^{-1})[a].

(v, γ) 1	(v', γ') 2	$\Omega(K, n\Gamma)$ 3	Value 4	(v, γ) 1	(v', γ') 2	$\Omega(K, n\Gamma)$ 3	Value 4
(0000, A_1)	(0000, A_1)	2(0, A_1)	2.695859440(30)		(0101, F_2)	3(1, F_1)10^4	−0.18456
	(0000, A_1)	4(0, A_1)10^4	−0.3341682		(0101, F_2)	3(3, F_1)10^4	−0.14931
	(0000, A_1)	4(4, A_1)10^5	−0.1547079	(0101, F_1)	(0002, A_1)	1(1, F_1)	0.0654326
	(0000, A_1)	6(0, A_1)10^8	0.114368	(0101, F_1)	(0002, E)	1(1, F_1)10^3	0.2570(29)
	(0000, A_1)	6(4, A_1)10^{10}	−0.51075	(0101, F_1)	(0002, F_2)	1(1, F_1)10^2	−0.13521(65)
	(0000, A_1)	6(6, A_1)10^{10}	−0.15638		(0002, F_2)	2(2, E)10^3	0.15454(15)
(0100, E)	(0100, E)	0(0, A_1)	929.9052358(36)		(0002, F_2)	2(2, F_2)10^5	0.1592
	(0100, E)	2(2, E)10^1	−0.10788392(27)		(0002, F_2)	3(1, F_2)10^5	−0.2948
	(0100, E)	3(3, A_2)10^4	0.2265992(77)		(0002, F_2)	3(3, A_2)10^5	0.3359
	(0100, E)	4(0, A_1)10^6	−0.4052		(0002, F_2)	3(3, F_1)10^5	−0.9951
	(0100, E)	4(2, E)10^6	−0.31077		(0002, F_2)	3(3, F_2)10^6	0.692
	(0100, E)	4(4, A_1)10^7	0.134	(0101, F_2)	(0002, A_1)	2(2, F_2)10^3	0.39137(18)
	(0100, E)	4(4, E)10^6	−0.12583		(0002, A_1)	3(3, F_2)10^5	−0.2096
(0100, E)	(0001, F_2)	1(1, F_1)	−4.5091962(17)	(0101, F_2)	(0002, E)	3(1, F_1)10^4	−0.14398(11)
	(0001, F_2)	2(2, F_2)	−0.021291586(93)	(0101, F_2)	(0002, F_2)	0(0, A_1)	−4.299716(92)
	(0001, F_2)	3(1, F_1)10^3	−0.1179753(12)		(0002, F_2)	1(1, F_1)	0.0257393(36)
	(0001, F_2)	3(3, F_2)10^4	0.136921(15)		(0002, F_2)	2(0, A_1)10^3	0.63439(11)
	(0001, F_2)	4(2, F_2)10^6	−0.212431(55)		(0002, F_2)	2(2, E)10^4	−0.2856
	(0001, F_2)	4(4, F_1)10^6	−0.18552		(0002, F_2)	3(1, F_1)10^5	−0.13438
	(0001, F_2)	4(4, F_2)10^6	−0.209879		(0002, F_2)	3(3, F_2)10^4	0.14725
	(0001, F_2)	5(1, F_1)10^8	−0.23013	(0002, A_1)	(0002, A_1)	0(0, A_1)	−13.0489115(82)
	(0001, F_2)	5(3, F_1)10^8	0.13677		(0002, A_1)	2(0, A_1)10^4	0.17329(66)
	(0001, F_2)	5(3, F_2)10^9	0.5885	(0002, A_1)	(0002, E)	2(2, E)10^3	0.215314(35)
(0001, F_2)	(0001, F_2)	0(0, A_1)	821.1167767(37)	(0002, A_1)	(0002, F_2)	2(2, F_2)10^3	−0.300740
	(0001, F_2)	1(1, F_1)	6.37846454(62)		(0002, F_2)	3(3, F_2)10^4	0.10079
	(0001, F_2)	2(0, A_1)10^2	0.1075775(30)	(0002, E)	(0002, E)	0(0, A_1)	1.4824568(99)
	(0001, F_2)	2(2, E)10^2	−0.1509974(27)		(0002, E)	2(2, E)10^3	−0.524940(86)
	(0001, F_2)	2(2, F_2)	−0.010699349(23)		(0002, E)	3(3, A_2)10^4	0.10591
	(0001, F_2)	3(1, F_1)10^4	0.702783(10)	(0002, E)	(0002, F_2)	1(1, F_1)	0.03030751(76)
	(0001, F_2)	3(3, F_1)10^4	−0.480174(11)		(0002, F_2)	2(2, F_2)10^3	−0.59961(10)
	(0001, F_2)	4(0, A_1)10^6	−0.370472(49)		(0002, F_2)	3(1, F_1)10^6	−0.3530
	(0001, F_2)	4(2, F_2)10^6	−0.3519		(0002, F_2)	3(3, F_1)10^5	−0.1960
	(0001, F_2)	4(4, A_1)10^7	−0.6407		(0002, F_2)	3(3, F_2)10^5	−0.5111
	(0001, F_2)	5(1, F_1)10^8	0.25953	(0002, F_2)	(0002, F_2)	0(0, A_1)	−1.244005(11)
	(0001, F_2)	5(3, F_1)10^8	−0.16967		(0002, F_2)	1(1, F_1)	−0.0327713(97)
	(0001, F_2)	6(0, A_1)10^{10}	0.4276		(0002, F_2)	2(0, A_1)10^4	−0.15486(60)
(0200, A_1)	(0200, A_1)	0(0, A_1)	−2.6836900		(0002, F_2)	2(2, E)10^3	0.1190
	(0200, A_1)	2(0, A_1)10^3	−0.4716		(0002, F_2)	2(2, F_2)10^3	0.58844
(0200, A_1)	(0200, E)	2(2, E)10^3	−0.259660		(0002, F_2)	3(1, F_1)10^6	−0.3567
(0200, E)	(0200, E)	0(0, A_1)	0.841533		(0002, F_2)	3(3, F_1)10^5	−0.5775
	(0200, E)	2(2, E)10^3	0.3393	(1000, A_1)	(1000, A_1)	0(0, A_1)	2110.7088020(33)
	(0200, E)	3(3, A_2)10^5	0.26045		(1000, A_1)	2(0, A_1)10^2	−1.7988113
(0200, A_1)	(0101, F_2)	2(2, F_2)10^3	−0.1180		(1000, A_1)	4(0, A_1)10^6	0.17727
(0200, E)	(0101, F_1)	1(1, F_1)	0.0267431		(1000, A_1)	4(4, A_1)10^8	−0.4386
	(0101, F_1)	2(2, F_2)10^3	−0.21017	(1000, A_1)	(0010, F_2)	2(2, F_2)10^2	−0.8100331(15)
	(0101, F_1)	3(3, F_2)10^5	−0.4234		(0010, F_2)	3(3, F_2)10^5	−0.175232(47)
(0200, E)	(0101, F_2)	1(1, F_1)	0.0317455		(0010, F_2)	4(2, F_2)10^6	−0.111586
	(0101, F_2)	3(1, F_1)10^5	−0.4543		(0010, F_2)	4(4, F_2)10^6	−0.158576
(0200, A_1)	(0002, A_1)	0(0, A_1)	−5.45804		(0010, F_2)	5(5, F_2)10^9	0.2873
	(0002, A_1)	2(0, A_1)10^3	0.52441	(0010, F_2)	(0010, F_2)	0(0, A_1)	2111.5739400(26)
(0200, E)	(0002, E)	0(0, A_1)	0.183116(88)		(0010, F_2)	1(1, F_1)	−0.55568226(53)
	(0002, E)	2(2, E)10^3	0.46393		(0010, F_2)	2(0, A_1)	−0.0147050657(76)
(0200, E)	(0002, F_2)	1(1, F_1)	0.230446(11)		(0010, F_2)	2(2, E)10^2	0.2275549(30)
	(0002, F_2)	3(1, F_1)10^5	−0.3016		(0010, F_2)	2(2, F_2)10^2	−0.4470184(17)
(0101, F_1)	(0101, F_1)	0(0, A_1)	2.2676814(70)		(0010, F_2)	3(1, F_1)10^5	−0.745775(61)
	(0101, F_1)	1(1, F_1)	−0.0510585(16)		(0010, F_2)	3(3, F_1)10^5	−0.65737
	(0101, F_1)	2(0, A_1)10^5	−0.5090		(0010, F_2)	4(0, A_1)10^8	0.3970
	(0101, F_1)	2(2, F_2)10^3	−0.7694		(0010, F_2)	4(2, E)10^7	0.93688(26)
(0101, F_1)	(0101, F_2)	1(1, F_1)	−0.0565839(28)		(0010, F_2)	4(2, F_2)10^7	−0.6775
	(0101, F_2)	2(2, E)10^4	0.7774		(0010, F_2)	4(4, A_1)10^7	0.10694
	(0101, F_2)	2(2, F_2)10^3	0.78652(11)		(0010, F_2)	4(4, E)10^7	0.1407
	(0101, F_2)	3(1, F_1)10^5	−0.58181		(0010, F_2)	4(4, F_2)10^6	−0.20740
(0101, F_2)	(0101, F_2)	0(0, A_1)	−2.0142367(99)		(0010, F_2)	5(1, F_1)10^9	−0.558
	(0101, F_2)	1(1, F_1)	−0.0552084(98)		(0010, F_2)	5(3, F_1)10^9	−0.18787
	(0101, F_2)	2(0, A_1)10^3	−0.37902		(0010, $1F_2$)	5(5, F_1)10^9	0.34126
	(0101, F_2)	2(2, E)10^3	0.3357		(0010, $3F_2$)	5(5, F_1)10^9	−0.66037
	(0101, F_2)	2(2, F_2)10^3	−0.8515				

[a] Values in parentheses are 1σ statistical confidence intervals. Parameters presented without confidence intervals were constrained to the values of corresponding parameters of the $^{73}GeH_4$ isotopologue from Ref. [1].

troscopic parameters for the effective Hamiltonian, [17–21]:

$$H^{vib.-rot.} = \sum_{\nu\gamma,\nu'\gamma'}\sum_{n\Gamma}[(|\nu\gamma\rangle\otimes\langle\nu'\gamma'|)^{n\Gamma}\otimes H^{n\Gamma}_{\nu\gamma,\nu'\gamma'}]^{A_1} \equiv \sum_{\nu\gamma,\nu'\gamma'}\sum_{n\Gamma}\sum_{\Omega K}[(|\nu\gamma\rangle\otimes\langle\nu'\gamma'|)^{n\Gamma}\otimes R^{\Omega(K,n\Gamma)}]^{A_1}Y^{\Omega(K,n\Gamma)}_{\nu\gamma,\nu'\gamma'}, \quad (2)$$

where $|\nu\gamma\rangle$ are the symmetrized vibrational functions, γ are symmetries of these functions; $R^{\Omega(K,n\Gamma)}_{\sigma}$ are symmetrized rotational operators, and Ω is the total degree of the rotational operators J_α ($\alpha = x, y, z$) in the individual operator R; K is the rank of this operator, Γ is its symmetry in the T_d point symmetry group, and n distinguishes between possible different operators $R^{\Omega(K,n\Gamma)}_{\sigma}$ having the same values of Ω, K and Γ (see, e.g., [22–25]). The sign $\otimes$ denotes a tensorial product, and the values $Y^{\Omega(K,n\Gamma)}_{\nu\gamma,\nu'\gamma'}$ are different–type spectroscopic parameters (for more details, see [1]).

The results of the fit are presented in column 4 of Table 3 together with their 1σ confidence statistical intervals (the latter are given in parentheses). Parameters in Table 3 (notations of parameters correspond to the notation of Ref. [21]), which are shown without parentheses, have been constrained to the corresponding values of parameters of the $^{73}GeH_4$ species from [1]. Correctness of the obtained results is confirmed by the fact that 53 parameters, obtained from the fit in the present study, reproduce the 9112 initial experimental line positions with the $d_{rms} = 2.44\times10^{-4}$ cm^{-1}. Column 5 of the Supplementary materials I, II and III presents the values of differences $\delta = (\nu^{exp.} - \nu^{calc.})$ in units of 10^{-4} cm^{-1} between the experimental line positions and the ones calculated with the parameters from Table 3. Fig. 5 shows the fitting statistics for the studied bands. As one more confirmation of the correctness of the results obtained, the lower parts of Figs. 1–3 and Fig. 4 a show spectra which were simulated with the parameters obtained in the present paper and correspond to the experimental spectra presented in the upper parts of Figs. 1–3 and 4b. Relative line strengths were calculated for the simulated spectra in Figs. 1 and 2, and the effective dipole moment parameters from [14] were used for the calculation of the line strengths in the simulated spectra of Figs. 3 and 4b.

It is interesting to compare both the shifts of line positions and change of different spectroscopic parameters under transfer from one isotopologue of germane to another. In accordance with the results and deductions of the isotopic substitution theory (see, e.g., [26,27]), the lower the value $(\frac{m'-m}{m'})$ (here m and m' is the mass of atom before and after isotopic substitution), the more linearly the mentioned characteristics (shifts and changes) depend on the change of masses of the substituted atoms. For the germane molecule the value $(\frac{m'-m}{m'})$ is changed in limits of $\left(\frac{1}{80}\div\frac{1}{20}\right)$. As a consequence, the mentioned rule should be applied with a high enough accuracy for this molecule. As an illustration, the parts 4b–d of Fig. 4 presents one of the experimentally recorded clusters for different germane species in the region of the R–branch. As one more illustration of the validity of the mentioned rule, Fig. 6 shows plots of the dependence of the values for some of the larger spectroscopic parameters of the isotopic species of germane (experimental data are taken from [1] and references cited therein). One can see a good confirmation of the above mentioned rule. This allows one to expect that this rule can be successfully applied to prediction of characteristics of other molecules on isotopic substitution of heavy enough atoms.

5. Conclusion

High resolution FTIR spectra of the $^{72}GeH_4$ molecule were recorded with a Bruker IFS 125HR Fourier transform spectrometer in the Dyad and Pentad regions. Ro–vibrational transitions belonging to the six "cold" (6761 transitions) and nine "hot" (2351 transitions) bands of $^{72}GeH_4$ were assigned in the experimental spectra. On that basis, 3817 ro–vibrational energies of the (0100, E), (0001, F_2), (1000, A_1), (0010, F_2), (0101, F_1), (0101, F_2), (0200, A_1), (0200, E), (0002, A_1), (0002, E), and (0002, F_2) vibrational bands were obtained and used in a weighted fitting procedure to determine the spectroscopic parameters of the effective Hamiltonian. A set of 53 parameters obtained from the fit reproduced the 3817 initial energy values (9112 line positions) with a $d_{rms} = 2.44\times10^{-4}$ cm^{-1}.

Acknowledgments

The work was funded by the Tomsk Polytechnic University Competitiveness Enhancement Program.

Supplementary material

Supplementary material associated with this article can be found, in the online version, at doi:10.1016/j.jqsrt.2018.12.036.

References

[1] Ulenikov ON, Gromova OV, Bekhtereva ES, Raspopova NI, Koshelev MA, Velmuzhova IA, Bulanov AD, Sennikov PG. High–resolution FTIR spectroscopic study of $^{73}GeH_4$ up to 2300 cm^{-1}. J Quant Spectrosc Radiat Transf 2018;221:129–37.
[2] Daunt SJ, Halsey GW, Fox K, Lovell RJ, Gailar NM. High-resolution infrared spectra of ν_3 and $2\nu_3$ of germane. J Chem Phys 1978;68:1319–21.
[3] Magerl G, Schupita W, Bonek E, Kreiner WA. Observation of the isotope effect in the ν_2 fundamental of germane. J Chem Phys 1980;72:395–8.
[4] Kreiner WA, Opferkuch R, Robiette AG, Turner PH. The ground–state rotational constants of germane. J Mol Spectrosc 1981;85:442–8.
[5] Lepage P, Champion JP, Robiette AG. Analysis of the ν_3 and ν_1 infrared bands of GeH_4. J Mol Spectrosc 1981;89:440–8.
[6] Zhu Q, Thrush BA, Robiette AG. Local mode rotational structure in the (3000) Ge-H stretching overtone ($3\nu_3$) of germane. Chem Phys Lett 1988;150:181–183.
[7] Zhu Q, Thrush BA. Rotational structure near the local mode limit in the (3000) band of germane. J Chem Phys 1990;92:2691–7.
[8] Zhu Q, Qian H, Thrush BA. Rotational analysis of the (2000) and (3000) bands and vibration-rotation interaction in germane local mode states. Chem Phys Lett 1991;186:436–40.
[9] Campargue A, Vetterhiiffer J, Chenevier M. Rotationally resolved overtone transitions of $^{70}GeH_4$ in the visible and near–infrared. Chem Phys Lett 1992;192:353–6.
[10] Permogorov D, Campargue A. The local mode model in silanes and germanes. Mol Phys 1997;92:117–25.
[11] Zhu Q, Campargue A, Vetterhöffer J, Permogorov D, Stoeckel F. High resolution spectra of GeH_4 $\nu = 6$ and 7 stretch overtones. the perturbed local mode vibrational states. J Chem Phys 1993;99:2359–64.
[12] Sun F, Wang X, Liao J, Zhu Q. The (5000) local mode vibrational state of germane: a high-resolution spectroscopic study. J Mol Spectrosc 1997;184:12–21.
[13] Chen XY, Lin H, Wang XG, Deng K, Zhu QS. High-resolution fourier transform spectrum of the (4000) local mode overtone of GeH_4: local mode effect. J Mol Struct 2000;517–518:41–51.
[14] Boudon V, Grigoryan T, Philipot F, Richard C, Tchana F, Manceron L, Rizopoulos A, Vander Auwera J, Encrenaz T. Line positions and intensities for the ν_3 band of 5 isotopologues of germane for planetary applications. J Quant Spectrosc Radiat Transf 2018;205:174–83.
[15] Gordon IE, Rothman LS, Hill C, Kochanov RV, Tan Y, Bernath PF, et al. The HITRAN 2016 molecular spectroscopic database. J Quant Spectrosc Radiat Transf 2017;203:3–69.
[16] Loéte M. Développement complet du moment dipolaire des molécules tétraédriques. application aux bandes triplement dégénérées et à la diade ν_2 et ν_4. Can J Phys 1983;61:1242–59.
[17] Moret-Bailly J. Sur l'interprétation des spectres de vibration-rotation des molécules à symétrie tétraédrique ou octaédrique. Cah Phys 1961;15:238–314.
[18] Champion JP, Pierre G, Michelot F, Moret-Bailly J. Composantes cubiques normales des tenseurs spheriques. Can J Phys 1977;55:512–20.
[19] Ulenikov ON. On the determination of the reduced rotational operator for polyatomic molecules. J Mol Spectrosc 1986;119:144–52.
[20] Champion JP. Developpement complet de l'hamiltonien de vibration-rotation adapté à1′étude des interactions dans les molécules toupies sphériques. Application aux bandes ν_2 et ν_4 de $^{12}CH_4$ Can J Phys 1977;55:1802–28.

[21] Boudon V, Champion JP, Gabard T, Loëte M, Michelot F, Pierre G, Rotger M, Wenger C, Rey M. Symmetry–adapted tensorial formalism to model rovibrational and rovibronic spectra of molecules pertaining to various point groups. J Mol Spectrosc 2004;228:620–34.
[22] Fano U, Racah G. Irreducible tensorial sets. New York: Academic Press; 1959.
[23] Varshalovitch DA, Moskalev AN, Khersonsky VK. Quantum theory of angular momentum. Leningrad: Nauka; 1975.
[24] Zhilinskii BI. Method of irreducible tensorial sets in molecular spectroscopy. Moscow: Moscow State University Press; 1981.
[25] Rey M, Boudon V, Wenger CH, Pierre G, Sartakhov B. Orientation of O(3) and SU(2)⊗C_I representation in cubic point groups (O_h, T_d) for application to molecular spectroscopy. J Mol Spectrosc 2003;219:313–25.
[26] Bykov AD, Makushkin Yu, Ulenikov ON. On isotope effect in polyatomic molecules. some comments on the method. J Mol Spectrosc 1981;85:462–479.
[27] Ulenikov ON, Bekhtereva ES, Onopenko GA, Sinitsin EA, Burger H, Jerzembeck W. Isotopic effects in XH_3 (C_{3v}) molecules: the lowest vibrational bands of PH_2D reinvestigated. J Mol Spectrosc 2001;208:236–48.